ACS APPLIED ENERGY MATERIALS

Article

Cite This: ACS Appl. Energy Mater. 2019, 2, 243−249

www.acsaem.org

Monolithic Perovskite/Silicon-Heterojunction Tandem Solar Cells with Open-Circuit Voltage of over 1.8 V

Fuhua Hou,† Lingling Yan,† Biao Shi,† Junfan Chen, Shijie Zhu, Qianshang Ren, Shichong An, Zhongxin Zhou, Huizhi Ren, Changchun Wei, Qian Huang, Guofu Hou, Xinliang Chen, Yuelong Li, Yi Ding, Guangcai Wang, Dekun Zhang, Ying Zhao, and Xiaodan Zhang*

Institute of Photoelectronic Thin Film Devices and Technology, Key Laboratory of Photoelectronic Thin Film Devices and Technology of Tianjin, Collaborative Innovation Center of Chemical Science and Engineering (Tianjin), Tianjin 300071, P. R. China

Supporting Information

ABSTRACT: Perovskite/silicon tandem solar cells with high theoretical efficiency, low cost, and the potential for simple mass production have received significant attention. To maintain the current matching, increasing the open-circuit voltage (V_{OC}) of the top and bottom subcells is an effective route to enhance the efficiency of tandem solar cells (TSCs). In this paper, we focus on a strategy for increasing the V_{OC} and simultaneously maintaining a high efficiency of over 20%. Perovskite thin films with added Cs in traditional FAMA cations have shown a large grain, smooth surface morphology, wider band gap, and reduced defects, which together bring about a TSC V_{OC} of 1.78 V. In addition, the high minority carrier lifetime (τ_{eff}) of bottom silicon solar cells resulting from the good passivation of a-Si:H/c-Si interface enhance the V_{OC} values to as high as 1.83 V, which is the highest value for perovskite/silicon TSCs.

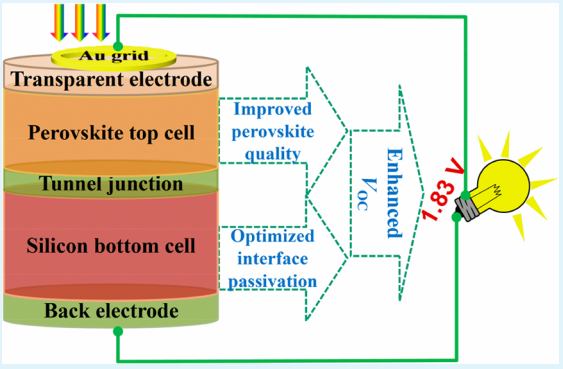

KEYWORDS: *perovskite/silicon tandem solar cells, high open-circuit voltage, Cs-doped perovskite film, silicon heterojunction, surface passivation, minority carrier lifetime*

1. INTRODUCTION

Emerging organic−inorganic hybrid perovskite solar cells (PSCs) differ from other photovoltaic devices as perfect top cell candidates for high-performance TSCs. Perovskite materials, promising solar cell absorbers with a large absorption coefficient, long carrier diffusion length, bipolar charge transport, and low exciton binding energy,[1−6] have allowed the efficiency of PSCs to reach over 22% after only a few years.[7−12]Moreover, attractive features of this material are the steep absorption edge and tunable band gap within the range of 1.48−2.23 eV, which can be better matched with the bottom cell.[13,14] Most importantly, the low-temperature solution processes imply that PSCs are an ideal choice for application to TSCs.[15] To achieve a full utilization of solar energy, crystalline silicon solar cells are excellent bottom cell candidates owing to their suitable band gap of 1.1 eV.[14] In addition, crystalline silicon solar cells based on intrinsic amorphous silicon (a-Si: H) passivation have a high V_{OC} of up to 750 mV,[16] an excellent near-infrared response, and high efficiency of over 26%.[17] Consequently, perovskite/silicon TSCs are expected to surpass the one junction Shockley-Queisser limit[18] and have already obtained 27.3% PCE that defeats the previous world record of a single junction silicon device.[19] Therefore, the establishment of an efficient perovskite/silicon tandem device is significant for the development of advanced photovoltaics.

The first perovskite/silicon TSC was reported by Mailoa et al., who connected a diffused junction silicon bottom cell with a mesoscopic perovskite top cell using a silicon tunneling recombination junction, and achieved a monolithic TSC with an efficiency of 13.7% and a modest V_{OC} of 1.58 V.[20] Driven by the modified deposition method and perovskite with mixed cations to improve the efficiency of the top cell and achieve better passivation of both sides of the c-Si subcell, the perovskite/homojunction-silicon was improved to 22.5% with a V_{OC} of 1.75 eV.[21] Compared with a diffused homojunction silicon solar cell, silicon heterojunction (SHJ) solar cells have a high V_{OC} because of the high-quality surface passivation induced by the intrinsic a-Si:H. Albrecht et al. employed a SHJ solar cell as the bottom cell for a two-terminal TSC, attaining a V_{OC} of 1.78 V and an efficiency of 19.9% by exploiting the high voltage potential.[22] The efficiency was further improved to 21.2% by carefully tuning the layer thickness to reduce any optical losses.[23] By tuning the perovskite band-gaps to realize

Received: June 7, 2018
Accepted: January 4, 2019
Published: January 4, 2019

DOI: 10.1021/acsaem.8b00926
ACS Appl. Energy Mater. 2019, 2, 243−249

Table 1. $J-V$ Characteristics of Perovskite/SHJ TSCs with and without Cs in Perovskite Film[a]

device	scan direction	J_{SC} (mV/cm^2)	V_{OC} (V)	FF	PCE (%)	Rs (Ω·cm^{-2})
control	reverse	15.11	1.73	0.69	18.08	14.35
	forward	15.09	1.73	0.70	18.35	11.44
Cs-doped	reverse	15.67	1.78	0.72	20.08	8.99
	forward	15.65	1.78	0.73	20.33	9.25

[a]All devices were measured using a 40 mV voltage step and 0.05 s delay time. "Reverse" indicates the scan direction from V_{OC} to J_{SC}, and "Forward" is from J_{SC} to V_{OC}.

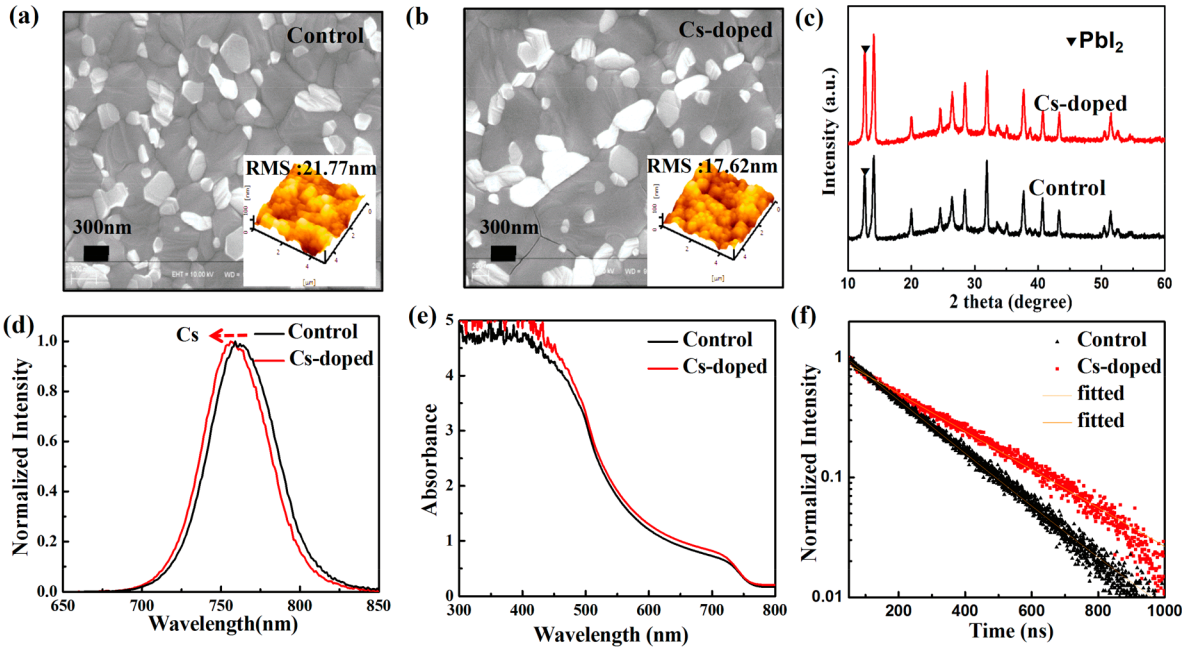

Figure 1. Top-view SEM images (the inset shows the AFM morphology) of the perovskite (a) without Cs addition and (b) with a Cs-doped film, and the (c) XRD spectra, (d) steady-state photoluminescence (PL) spectra, (e) absorbance spectra, and (f) TRPL spectra for a glass/perovskite film prepared with and without Cs added. Scale bars = 300 nm.

current matching with the bottom cells, Fan et al. achieved a PCE of 20.57% through the use of an all-solution process top cell.[24] Sahli et al. enhanced the performance to 22.7% by improving the light utilization with a nanocrystalline silicon recombination layer.[25] Through the delicate design of the device structure to reduce parasitic absorption, and applying textured silicon to enhance the absorption, Bush et al. obtained an efficiency level of 23.6% for a monolithic perovskite/silicon cell with a PIN configuration, the short-circuit current density (J_{SC}) of which can reach up to 18.1 mA/cm^2, with a V_{OC} of only 1.65 V.[26] The same group further optimized HTM and bandgap as well as reduced reflection to maximize the efficiency to 25.0%.[27] Sahli et al. used the double-side textured silicon to reduce the reflection loss and improve light trapping, achieving a certified efficiency of 25.2%.[28] In a monolithic tandem, the photocurrent is determined on the basis of the smaller photocurrent between the top and bottom cells, with V_{OC} being their sum. Although most studies have reported TSCs with an improved J_{SC}, little attention has been paid to the V_{OC}. On the premise of maintaining the current-matched, the V_{OC} is also an important factor in improving the ultimate level of efficiency. It has been deduced that the conversion efficiency of two-terminal perovskite/silicon TSCs will easily reach over 30% under the realistic assumption that the V_{OC}, J_{SC}, and FF for a PIN or NIP type tandem exceed 1.83 V, 20.5 mA/cm^2, and 80%, respectively.

In this study, we fabricated perovskite/SHJ monolithic TSCs under a low-temperature process, achieving a V_{OC} and efficiency of up to 1.83 V and 20.43% in the reverse scan direction, respectively. These performances were obtained through a design and performance enhancement of both the subcell of the perovskite and the silicon applied. We found that Cs-doped perovskite films will bring about an enhancement of V_{OC} for TSCs owing to the improvement of the surface morphology with larger grain sizes, reduced roughness, and widened band gap. Furthermore, our research showed that the minority carrier lifetime (τ_{eff}) of the bottom silicon solar cells also plays an essential role in obtaining a high V_{OC} for TSCs.

2. RESULTS AND DISCUSSION

In the construction of a monolithic perovskite/silicon TSC, the SHJ was employed as the bottom cell owing to its high V_{OC}. The performance of the top cell is beneficial for the overall tandem efficiency. The compositional engineering of mixed-cation perovskites is an effective method to achieve a more stable and high-level performance of perovskite solar cells. By adding Cs and Rb to better tune the Goldschmidt tolerance factor, a more stable perovskite solar cell was obtained.[29,30] Potassium was also introduced in perovskite with a better decorated surface and grain boundary.[31] McMeekin et al.[13] and Bush et al.[26] reported the use of FACs perovskite in tandem solar cells with better stability and performance. Specifically, a

DOI: 10.1021/acsaem.8b00926
ACS Appl. Energy Mater. 2019, 2, 243−249

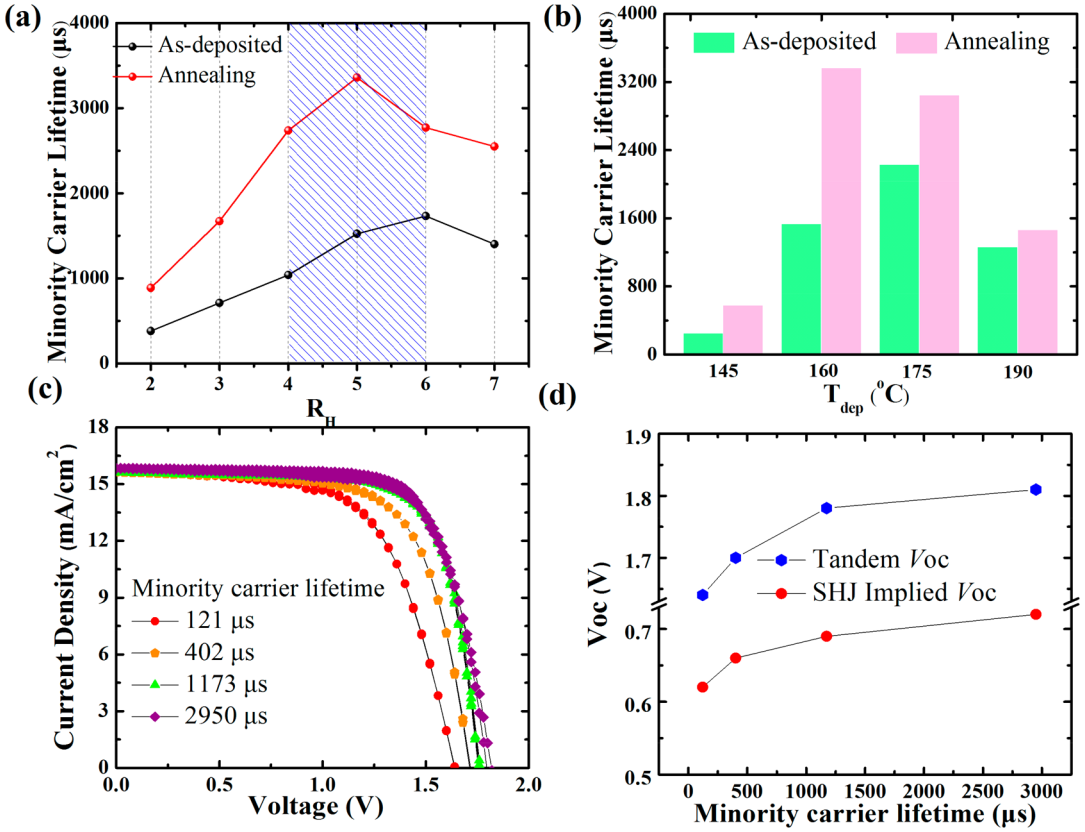

Figure 2. (a) Dependence of τ_{eff} on R_H with and without postannealing. (b) Measured τ_{eff} when varying the deposition temperature under deposited and postannealing while fixing the R_H at 5. The postannealing of the intrinsic a-Si:H thin films in this work was conducted at 200 °C for 30 min. (c) $J-V$ curves of perovskite/SHJ TSCs with τ_{eff} of 121, 402, 1173, and 2950 μs of the SHJ bottom cells. (d) The relationship between τ_{eff} and implied V_{OC} of SHJ and V_{OC} of the TSCs.

more efficient single junction perovskite solar cell was made using mostly FAMA perovskite; thus, FAMA-perovskite-based TSCs have greater potential to obtain a better performance and were therefore considered in the present study. Compared with our previous studies focusing on transparent electrode molybdenum oxide (MoOx)/ITO through an optimization of the sputtering power of the transparent electrode and the thickness of the MoOx buffer layer,[32] we further modified the two subcells of a perovskite/silicon TSC. In detail, we deposited the FAMA perovskite top cell onto the silicon bottom cell with a matched band gap, and we demonstrated an improved performance of the tandem cells after the addition of CsI. Although the changes in the minority carrier lifetime of a Si subcell as a function of the annealing temperature are well-known, it is worth mentioning that the current reports regarding perovskite/silicon tandem solar cells are not related to the optimization of the passivation layers for the bottom solar cells, which is one of the main factors limiting the efficiency of a TSC. Therefore, there is no doubt that optimizing the passivation layers is an effective method for gaining a high-performance TSC. In brief, it is the two subcells with a higher V_{OC} that have given rise to the highest V_{OC} of TSCs thus far. In this study, the structure of the perovskite top cell applied is SnO_2/perovskite/Spiro-OMeTAD/MoO_x/ITO. A SnO_2 electron-transporting layer was deposited as the solution process, achieving a better electron mobility and energy band matching with perovskite. MoO_X is used as a buffer layer to suppress damage to the sputtering transparent electrode ITO. We modified the quality of the FAMA perovskite through the addition of Cs. The FAMA perovskite precursor solution contained FAI (0.9 M), PbI_2 (1.1 M), MABr (0.3 M), and $PbBr_2$ (0.3 M), and for the FAMACs perovskite, CsI (0.1 M) was added while proportionally reducing the amount of FAI and MABr to keep the total amount of organic cations unchanged. Both perovskite materials were dissolved in anhydrous DMF/DMSO at a ratio of 4/1 (v/v). The device parameters are illustrated in Table 1, which shows that all parameters, including J_{SC}, V_{OC}, and FF, were clearly improved after the addition of CsI.

To demonstrate the functionality of Cs in the FAMA perovskite materials, we comprehensively studied FAMA and FAMACs perovskite in view of the film morphology, crystal phase, and defect property as follows. A top-view SEM image of the Cs-doped perovskite films showed better crystal morphologies, with grain sizes reaching ~800 nm compared with ~400 nm of the control films (Figure 1a,b). The modified morphology may be attributed to the small amount of Cs acting as nucleation sites and inducing larger and more monolithic vertical perovskite crystals.[33] In addition, the reduced grain boundaries lead to a high V_{OC} and J_{SC} for the low defect states.[34,35] The Cs-doped perovskite film became denser and smoother, as indicated by the AFM morphology (inset of Figure 1a,b). The roughness of the Cs-doped perovskite films was 17.60 nm, in contrast to 21.77 nm of the control films, within a scanning range of 5 μm × 5 μm. It is thought that the smooth surface can supply the perovskite layer with a better interfacial contact with the Spiro-OMeTAD

DOI: 10.1021/acsaem.8b00926
ACS Appl. Energy Mater. 2019, 2, 243−249

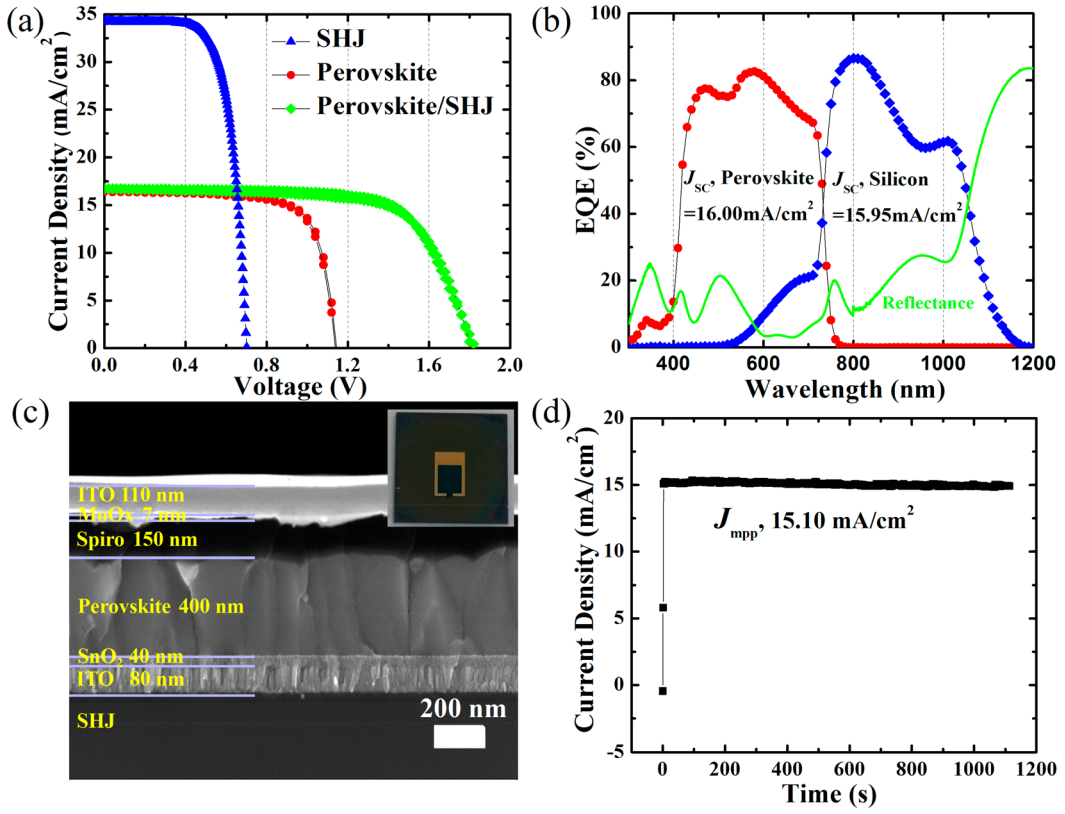

Figure 3. (a) $J-V$ curves of the semitransparent PSC, silicon single solar cell, and champion TSC with a dual sweep. (b) External quantum efficiency (EQE) of the top and bottom subcells in the monolithic TSC and the corresponding integrated reflectance. (c) Cross-sectional SEM image of the tandem device (the inset shows the top view of an actual device with an active area of 0.13 cm^2). (d) The steady-state output current during 1000 s of maximum power point tracking of the best two-terminal perovskite/SHJ tandem device.

HTL, resulting in a reduced series resistance and an improved fill factor (FF).[36]

The XRD results (Figure 1c) and the bright spots in the SEM images of both samples indicate the presence of PbI_2, which has a positive passivation effect and is thus beneficial for enhancing the performance of the devices.[36−39] The Cs-doped perovskite film showed a higher intensity of 14.0 degrees compared to the control film, indicating a high perovskite crystalline quality, which was better confirmed through the SEM results. It should be mentioned that the amount of residual PbI_2 in the film was not reduced, mainly because we kept the ratio of the total amount of organic cations and PbI_2 unchanged with and without the use of Cs-doped films. The photoluminescence (PL) spectra of the Cs-doped films shown in Figure 1d was blue-shifted by 7 nm compared to the reference, indicating that the addition of Cs slightly enlarged the band gap, thereby leading to a higher V_{OC}.[31] Consequently, the band gap of the Cs-doped perovskite is ∼1.67 eV, the current of which can be better matched with the silicon bottom cell in the presence of parasitic absorption.

The Cs-containing film displayed a larger absorbance than the FAMA film because of the larger grain size and improved crystallinity of the Cs-doped film (Figure 1e). The improved absorbance of the Cs-doped film can be better explained by the increase in the current density, as indicated in Table 1. To further investigate the charge recombination behavior after Cs added to the FAMA perovskite film, the time-resolved photoluminescence (TRPL) was measured. We used a single exponential decay model to fit the PL decay curves, namely, $I(t) = I_0 \exp(-t/\tau)$, where τ is the lifetime and I_0 is the intensity at time zero (upon excitation). The carrier lifetime of Cs-doped film was prolonged to 274.0 ns, as compared to the 194.6 ns of a pristine film. This indicates a reduced defect concentration and results in a superior electronic quality for the Cs-doped perovskite film, which again accounts for the higher V_{OC} of the Cs-added devices. As a whole, adding Cs to a perovskite precursor solution can boost the V_{OC} of the TSC from 1.73 to 1.78 V, and the efficiency from 18.35% to 20.33%.

To achieve a high efficiency of the silicon bottom cell, a surface passivation of the crystalline silicon should be carried out.[40] It is commonly believed that the key issue is the chemical passivation of the Si dangling bonds (DBs) by the hydrogen at the a-Si:H/c-Si interface.[41] In consideration of the surface passivation, we concentrated on a modification of the intrinsic a-Si:H thin film by independently changing the hydrogen dilution ratio and substrate temperature. The correlation curves of the passivation quality with and without postannealing (200 °C for 30 min) for the dilution ratio of hydrogen to silane R_H ($R_H = [H_2]/[SiH_4]$) is illustrated in Figure 2a. In the case of R_H of ∼5, the lifetime reached its peak. In general, information regarding the passivation quality of the a-Si:H film can be deduced from the high stretching mode (HSM) and low stretching mode (LSM). Usually, the LSM is assigned to the vibration of monohydrides (Si−H), which represents a compact incorporation of hydrogen, whereas the HSM is attributed to higher hydrides (SiH_2) associated with large voids in the bulk material. During the annealing treatment, the hydrogen is released when the SiH_2 is transformed into a Si−H configuration. The reorganization of the hydrogen at the a-Si:H/c-Si interface (migration from

DOI: 10.1021/acsaem.8b00926
ACS Appl. Energy Mater. 2019, 2, 243−249

the bulk to the interface) then saturates the defects at the a-Si:H/c-Si interface, improving the passivation performance.[41,42] With a fixed R_H of 5, a high τ_{eff} can be obtained by adjusting the substrate temperature, as described in Figure 2b. Clearly, the τ_{eff} of the as-deposited sample indicates an increasing trend with the variation in the substrate temperature from 145 to 175 °C. The lifetime then reaches saturation at 175 °C and decreases with an increase in the deposition temperature to up to 190 °C. With a postannealing treatment, the lifetime of all samples was increased, which indicates that no epitaxial growth occurred.[38]

Figure 2c shows the $J-V$ curves for perovskite/SHJ when varying τ_{eff} of the silicon bottom cells obtained at various deposition temperatures, and the corresponding device parameters listed in Table S1. With an improvement in τ_{eff}, the V_{OC} of the TSCs showed a monotonous increase, from 1.62 to 1.81 V, and the FF showed an increasing trend initially, and reached a level of saturation, whereas the J_{SC} was similar for all devices. The implied V_{OC} is the theoretical maximum open-circuit voltage,[17] and a good interface passivation with a high τ_{eff} can reduce the carrier recombination and increase the V_{OC} and FF of the silicon bottom cell[40] and hence the performance of the TSCs. As shown in Figure 2d, when τ_{eff} was 121, 402, 1173, and 2950 μs, an implied V_{OC} of 0.62, 0.66, 0.69, and 0.72 V was obtained, respectively, corresponding to a V_{OC} of 1.62, 1.71, 1.78, and 1.81 V for the TSCs.

Knowing the relationship between V_{OC} and τ_{eff}, with a high τ_{eff} of the bottom cell and optimized perovskite top cell, a higher V_{OC} of the TSCs can be obtained. Figure 3a shows the $J-V$ curves of a single-junction semitransparent perovskite solar cell, silicon heterojunction solar cell, and the champion monolithic TSCs in both scan directions. The device parameters extracted from the $J-V$ curves are listed in Table 2. The semitransparent perovskite top cells fabricated on glass/ITO substrates achieved a V_{OC} of 1.18 V, together with an FF of 0.70 and a J_{SC} of 19.12 mA/cm^2, resulting in a PCE of 15.79%, and showing negligible hysteresis. The high V_{OC} of the PSC is a key factor in obtaining a high V_{OC} of the ultimate TSC. Meanwhile, a good passivation of the SHJ was achieved with a V_{OC} of 0.70 V, which is nearly 25 mV lower than the implied V_{OC}. Combining the efficient and stable perovskite solar cell with the better surface passivation of the SHJ, we fabricated monolithic TSCs with an efficiency of 21.31% in the reverse scan direction, with a V_{OC} of 1.83 V, J_{SC} of 16.74 mA/cm^2, and FF of 0.70. This is the highest V_{OC} for perovskite/SHJ TSCs reported thus far (Table S2). The cell performance showed negligible hysteresis with a slightly lower efficiency of 20.79% in the forward scan direction, with a V_{OC} of 1.81 V, J_{SC} of 16.70 mA/cm^2, and FF of 0.70. As shown in Figure 3b, the integrated J_{SC} from EQE was 16.00 mA/cm^2 for the perovskite top cell, and 15.95 mA/cm^2 for the silicon bottom cell. In the two-terminal TSC, before being absorbed at the perovskite layer, light first passed through the transparent electrode and the HTL layer. Doped Spiro-OMeTAD HTL has an observable parasitic absorption mainly in the blue wavelength range,[22] which explains the phenomenon of a low EQE response below a wavelength of 400 nm. In addition, the reflectance within the wavelength range of 900−1000 nm was large, corresponding to the low EQE response, which can be partly attributed to the refractive index mismatch between the crystalline silicon ($n_{c\text{-}Si}$ = 3.6−3.7 at 900 nm) and ITO recombination (n_{ITO} = 1.6−2.0 at 900 nm, depending on its doping).[43] The similar EQE curves can be found in the reports of tandem device using double-side polished silicon bottom cell.[23,24] Additionally, the peak of EQE curves of tandem device can be reshaped as a function of ITO thickness.[32] In order to minimize the reflection loss, a better refractive index-matched nanocrystalline silicon recombination junction replaced TCO[25] and textured silicon solar cells[27,28] have been applied in TSCs. It should be noted that there is a 4.7% discrepancy between the J_{SC} obtained from the $J-V$ measurement and the integrated J_{SC} from the EQE results for the tandem cell in the reverse scan direction. An overestimation of J_{SC} may occur in perovskite and perovskite/silicon solar cells.[25,44,45] This phenomenon can be attributed to the aperture of the "metal mask" being slightly larger than the active area of the TSC in the previous measurement. To more accurately evaluate the efficiency, the integrated current from the EQE was used to replace the current directly extracted from the $J-V$ curves. The ultimate calibration efficiency of the TSC was 20.43% in the reverse scan direction, and 19.91% in the forward scan direction. In our NIP configuration, the relatively low J_{SC} is due to the strong parasitic absorption of Spiro-OMeTAD, the high reflectance of the planar front surface, and the lack of an appropriate antireflection coating. The certified 23.6% PIN type tandem cells have a high J_{SC} of 18.1 mA/cm^2 because of the circumvention of parasitic absorption when selecting a less parasitic absorption PCBM or SnO_2 as electron-transporting layer, and rear textured silicon to elongate its path length. In the following work, we will focus on improving the J_{SC} through the introduction of a novel HTL with less parasitic absorption, an antireflection foil, and a light trapping structure. Additionally, the V_{OC} of our result is over 1.8 V, which is due to the optimized band alignments between the perovskite and ETL or HTL, and the better passivation of the silicon bottom cell.

Figure 3c shows a cross-sectional SEM image of the TSC structure. Each layer of the perovskite top cell can be clearly seen, as can the silicon wafer at the bottom of the image. The layer of the perovskite is nearly composed of single perovskite crystals with a size of about 400 nm. Spiro-OMeTAD was deposited uniformly on the perovskite film with a thickness of 150 nm. Then, 9 nm of MoO_x was slowly evaporated on top of the Spiro-OMeTAD to reduce any damage from the sputtering of the 110 nm ITO transparent electrodes. The stability of the TSCs was monitored by keeping the devices under continuous

Table 2. $J-V$ Parameters for a Semitransparent PSC (ST-PSC), a Silicon Heterojunction (SHJ) Solar Cell, and the Optimal Perovskite/SHJ TSC[a]

device	scan direction	J_{SC} (mV/cm^2)	V_{OC} (V)	FF	PCE (%)
ST-PSC	reverse	16.39	1.14	0.74	13.83
rear illum.	forward	16.38	1.14	0.73	13.63
ST-PSC	reverse	19.12	1.18	0.70	15.79
front illum.	forward	19.10	1.18	0.70	15.78
SHJ	forward	34.22	0.70	0.70	16.83
TSC	reverse	16.74	1.83	0.70	21.31
	forward	16.70	1.81	0.69	20.79
TSC (calibration from EQE)	reverse	15.95	1.83	0.70	20.43
	forward	15.95	1.81	0.69	19.91

[a]"rear illum." is defined as illumination from the HTL side, whereas "front illum." indicates illumination from the glass/ITO side. All devices were tested without an antireflective layer.

DOI: 10.1021/acsaem.8b00926
ACS Appl. Energy Mater. 2019, 2, 243−249

soaking of simulated AM 1.5 sunlight for nearly 20 min, and as demonstrated in Figure 3d, the J_{mpp} was maintained at 15.10 mA/cm^2 with no decline.

3. CONCLUSIONS

To summarize, we reported high-performance TSCs obtained through the component control of a perovskite film at the top cell and interface passivation of HIT at the bottom cell. The Cs-doped perovskite film can modify the surface morphology with a larger grain size and reduced surface roughness compared to the FAMA control film. The boosting of V_{OC} for Cs-containing devices was due to the widened band gap and reduced trap density. Meanwhile, a high V_{OC} related to the minority carrier lifetimes of the silicon bottom cells was achieved through an optimization of the hydrogen-to-silane dilution ratio, R_H, and the substrate temperature during deposition of the intrinsic a-Si:H layer. As a result, we achieved monolithic perovskite/SHJ TSCs with a maximum V_{OC} of up to 1.83 V and a power-conversion efficiency of 20.43% in the reserve scan direction without any light trapping. To the best of our knowledge, the V_{OC} obtained in this study is the highest value for TSCs thus far obtained. TSCs with a high V_{OC} and simultaneously high efficiency demonstrate a very significant perspective for application in special electronics devices, solar fuels, and other applications.

■ ASSOCIATED CONTENT

Supporting Information

The Supporting Information is available free of charge on the ACS Publications website at DOI: 10.1021/acsaem.8b00926.

Detailed description of materials preparations, device fabrications, characterization methods, $J-V$ parameters for TSCs with minority carrier lifetimes from 121 to 2950 μs of SHJ solar cells, comparison the device parameters of monolithic perovskite/silicon tandem between literatures and this work (PDF)

■ AUTHOR INFORMATION

Corresponding Author

*E-mail: xdzhang@nankai.edu.cn. Tel.: +86-22-23499304. Fax: +86 22-23499304.

ORCID

Yuelong Li: 0000-0003-0168-6107

Xiaodan Zhang: 0000-0002-0522-5052

Author Contributions

†(F.H., L.Y., B.S.) These authors contributed equally to this study. F.H., X.Z. conceived the study. F.H., L.Y., B.S., J.C., S.Z., Q.R., S.A., Z.Z., H.R., carried out the experiments. F.H. wrote the manuscript. X.Z., Y.Z. supervised the project. All authors discussed the results and implications and commented on the manuscript at all stages.

Notes

The authors declare no competing financial interest.

■ ACKNOWLEDGMENTS

The authors gratefully acknowledge the supports from National Natural Science Foundation of China (61474065 and 61674084), Tianjin Research Key Program of Science and Technology (18ZXJMTG00220), 111 Project (B16027), and Fundamental Research Funds for the Central Universities.

■ REFERENCES

(1) Xing, G.; Mathews, N.; Sun, S.; Lim, S. S.; Lam, Y. M.; Gratzel, M.; Mhaisalkar, S.; Sum, T. C. Long-Range Balanced Electron- and Hole-Transport Lengths in Organic-Inorganic $CH_3NH_3PbI_3$. *Science* **2013**, *342*, 344−347.

(2) Shi, D.; Adinolfi, V.; Comin, R.; Yuan, M.; Alarousu, E.; Buin, A.; Chen, Y.; Hoogland, S.; Rothenberger, A.; Katsiev, K.; Losovyj, Y.; Zhang, X.; Dowben, P. A.; Mohammed, O. F.; Sargent, E. H.; Bakr, O. M. Low Trap-State Density and Long Carrier Diffusion in Organolead Trihalide Perovskite Single Crystals. *Science* **2015**, *347*, 519−522.

(3) Stranks, S. D.; Eperon, G. E.; Grancini, G.; Menelaou, C.; Alcocer, M. J. P.; Leijtens, T.; Herz, L. M.; Petrozza, A.; Snaith, H. J. Electron-Hole Diffusion Lengths Exceeding 1 Micrometer in an Organometal Trihalide Perovskite Absorber. *Science* **2013**, *342*, 341−344.

(4) Choi, J. J.; Yang, X.; Norman, Z. M.; Billinge, S. J. L.; Owen, J. S. Structure of Methylammonium Lead Iodide Within Mesoporous Titanium Dioxide: Active Material in High-Performance Perovskite Solar Cells. *Nano Lett.* **2014**, *14*, 127−133.

(5) Wehrenfennig, C.; Eperon, G. E.; Johnston, M. B.; Snaith, H. J.; Herz, L. M. High Charge Carrier Mobilities and Lifetimes in Organolead Trihalide Perovskites. *Adv. Mater.* **2014**, *26*, 1584−1589.

(6) Marchioro, A.; Teuscher, J.; Friedrich, D.; Kunst, M.; van de Krol, R.; Moehl, T.; Grätzel, M.; Moser, J. E. Unravelling the Mechanism of Photoinduced Charge Transfer Processes in Lead Iodide Perovskite Solar Cells. *Nat. Photonics* **2014**, *8*, 250−255.

(7) Kojima, A.; Teshima, K.; Shirai, Y.; Miyasaka, T. Organometal Halide Perovskites as Visible-Light Sensitizers for Photovoltaic Cells. *J. Am. Chem. Soc.* **2009**, *131*, 6050−6051.

(8) Im, J. H.; Lee, C. R.; Lee, J. W.; Park, S. W.; Park, N. G. 6.5% Efficient Perovskite Quantum-Dot-Sensitized Solar Cell. *Nanoscale* **2011**, *3*, 4088−4093.

(9) Yang, W. S.; Noh, J. H.; Jeon, N. J.; Kim, Y. C.; Ryu, S.; Seo, J.; Seok, S. II. High-Performance Photovoltaic Perovskite Layers Fabricated through Intramolecular Exchange. *Science* **2015**, *348*, 1234−1237.

(10) Kim, H. S.; Lee, C. R.; Im, J. H.; Lee, K. B.; Moehl, T.; Marchioro, A.; Moon, S. J.; Humphry-Baker, R.; Yum, J. H.; Moser, J. E.; Grätzel, M.; Park, N.-G. Lead Iodide Perovskite Sensitized All-Solid-State Submicron Thin Film Mesoscopic Solar Cell with Efficiency Exceeding 9%. *Sci. Rep.* **2012**, *2*, 591.

(11) Yang, W. S.; Park, B. W.; Jung, E. H.; Jeon, N. J.; Kim, Y. C.; Lee, D. U.; Shin, S. S.; Seo, J.; Kim, E. K.; Noh, J. H.; Seok, S. II. Iodide Management in Formamidinium-Lead-Halide−Based Perovskite Layers for Efficient Solar Cells. *Science* **2017**, *356*, 1376−1379.

(12) Tan, H.; Jain, A.; Voznyy, O.; Lan, X.; Garcia de Arquer, F. P.; Fan, J. Z.; Quintero-Bermudez, R.; Yuan, M.; Zhang, B.; Zhao, Y.; Fan, F.; Li, P.; Quan, L. N.; Zhao, Y.; Lu, Z. H.; Yang, Z.; Hoogland, S.; Sargent, E. H. Efficient and Stable Solution-Processed Planar Perovskite Solar Cells via Contact Passivation. *Science* **2017**, *355*, 722−726.

(13) McMeekin, D. P.; Sadoughi, G.; Rehman, W.; Eperon, G. E.; Saliba, M.; Horantner, M. T.; Haghighirad, A.; Sakai, N.; Korte, L.; Rech, B.; Johnston, M. B.; Herz, L. M.; Snaith, H. J. A Mixed-Cation Lead Mixed-Halide Perovskite Absorber for Tandem Solar Cells. *Science* **2016**, *351*, 151−155.

(14) Shah, A.; Torres, P.; Tscharner, R.; Wyrsch, N.; Keppner, H. Photovoltaic Technology: The Case for Thin-Film Solar Cells. *Science* **1999**, *285*, 692−698.

(15) Fu, F.; Feurer, T.; Jäger, T.; Avancini, E.; Bissig, B.; Yoon, S.; Buecheler, S.; Tiwari, A. N. Low-Temperature-Processed Efficient Semi-Transparent Planar Perovskite Solar Cells for Bifacial and Tandem Applications. *Nat. Commun.* **2015**, *6*, 8932.

(16) Taguchi, M.; Yano, A.; Tohoda, S.; Matsuyama, K.; Nakamura, Y.; Nishiwaki, T.; Fujita, K.; Maruyama, E. 24.7% Record Efficiency HIT Solar Cell on Thin Silicon Wafer. *IEEE J. Photovoltaics* **2014**, *4*, 96−99.

(17) Yoshikawa, K.; Kawasaki, H.; Yoshida, W.; Irie, T.; Konishi, K.; Nakano, K.; Uto, T.; Adachi, D.; Kanematsu, M.; Uzu, H.; Yamamoto,

K. Silicon Heterojunction Solar Cell with Interdigitated Back Contacts for a Photoconversion Efficiency Over 26%. *Nat. Energy* **2017**, *2*, 17032.
(18) Filipič, M.; Löper, P.; Niesen, B.; Wolf, S. D.; Krč, J.; Ballif, C.; Topi, M. $CH_3NH_3PbI_3$ Perovskite/Silicon Tandem Solar Cells: Characterization based Optical Simulations. *Opt. Express* **2015**, *23*, 263−278.
(19) *Oxford PV sets world record for perovskite solar cell*. See the following: https://www.oxfordpv.com/news/oxford-pv-sets-world-record-perovskite-solar-cell, 2018.
(20) Mailoa, J. P.; Bailie, C. D.; Johlin, E. C.; Hoke, E. T.; Akey, A. J.; Nguyen, W. H.; McGehee, M. D.; Buonassisi, T. A 2-Terminal Perovskite/Silicon Multijunction Solar Cell Enabled by a Silicon Tunnel Junction. *Appl. Phys. Lett.* **2015**, *106*, 121105.
(21) Wu, Y.; Yan, D.; Peng, J.; Duong, T.; Wan, Y.; Phang, S. P.; Shen, H.; Wu, N.; Barugkin, C.; Fu, X.; Surve, S.; Grant, D.; Walter, D.; White, T. P.; Catchpole, K. R.; Weber, K. J. Monolithic Perovskite/Silicon-Homojunction Tandem Solar Cell with over 22% Efficiency. *Energy Environ. Sci.* **2017**, *10*, 2472−2479.
(22) Albrecht, S.; Saliba, M.; Correa Baena, J. P.; Lang, F.; Kegelmann, L.; Mews, M.; Steier, L.; Abate, A.; Rappich, J.; Korte, L.; Schlatmann, R.; Nazeeruddin, M. K.; Hagfeldt, A.; Grätzel, M.; Rech, B. Monolithic Perovskite/Silicon-Heterojunction Tandem Solar Cells Processed at Low Temperature. *Energy Environ. Sci.* **2016**, *9*, 81−88.
(23) Werner, J.; Weng, C. H.; Walter, A.; Fesquet, L.; Seif, J. P.; De Wolf, S.; Niesen, B.; Ballif, C. Efficient Monolithic Perovskite/Silicon Tandem Solar Cell with Cell Area > 1 cm^2. *J. Phys. Chem. Lett.* **2016**, *7*, 161−166.
(24) Fan, R.; Zhou, N.; Zhang, L.; Yang, R.; Meng, Y.; Li, L.; Guo, T.; Chen, Y.; Xu, Z.; Zheng, G.; Huang, Y.; Li, L.; Qin, L.; Qiu, X.; Chen, Q.; Zhou, H. Toward Full Solution Processed Perovskite/Si Monolithic Tandem Solar Device with PCE Exceeding 20%. *Solar RRL* **2017**, *1*, 1700149.
(25) Sahli, F.; Kamino, B. A.; Werner, J.; Bräuninger, M.; Paviet-Salomon, B.; Barraud, L.; Monnard, R.; Seif, J. P.; Tomasi, A.; Jeangros, Q.; Hessler-Wyser, A.; De Wolf, S.; Despeisse, M.; Nicolay, S.; Niesen, B.; Ballif, C. Improved Optics in Monolithic Perovskite/Silicon Tandem Solar Cells with a Nanocrystalline Silicon Recombination Junction. *Adv. Energy Mater.* **2018**, *8*, 1701609.
(26) Bush, K. A.; Palmstrom, A. F.; Yu, Z. J.; Boccard, M.; Cheacharoen, R.; Mailoa, J. P.; McMeekin, D. P.; Hoye, R. L. Z.; Bailie, C. D.; Leijtens, T.; Peters, I. M.; Minichetti, M. C.; Rolston, N.; Prasanna, R.; Sofia, S.; Harwood, D.; Ma, W.; Moghadam, F.; Snaith, H. J.; Buonassisi, T.; Holman, Z. C.; Bent, S. F.; McGehee, M. D. 23.6%-Efficient Monolithic Perovskite/Silicon Tandem Solar Cells with Improved Stability. *Nat. Energy* **2017**, *2*, 17009.
(27) Bush, K. A.; Manzoor, S.; Frohna, K.; Yu, Z. J.; Raiford, J. A.; Palmstrom, A. F.; Wang, H.-P.; Prasanna, R.; Bent, S. F.; Holman, Z. C.; McGehee, M. D. Minimizing Current and Voltage Losses to Reach 25% Efficient Monolithic Two-Terminal Perovskite−Silicon Tandem Solar Cells. *ACS Energy Lett.* **2018**, *3*, 2173−2180.
(28) Sahli, F.; Werner, J.; Kamino, B. A.; Bräuninger, M.; Monnard, R.; Paviet-Salomon, B.; Barraud, L.; Ding, L.; Diaz Leon, J. J.; Sacchetto, D.; Cattaneo, G.; Despeisse, M.; Boccard, M.; Nicolay, S.; Jeangros, Q.; Niesen, B.; Ballif, C. Fully Textured Monolithic Perovskite/Silicon Tandem Solar Cells with 25.2% Power Conversion Efficiency. *Nat. Mater.* **2018**, *17*, 820−826.
(29) Saliba, M.; Matsui, T.; Seo, J.-Y.; Domanski, K.; Correa-Baena, J. P.; Nazeeruddin, M. K.; Zakeeruddin, S. M.; Tress, W.; Abate, A.; Hagfeldt, A.; Gratzel, M. Cesium-Containing Triple Cation Perovskite Solar Cells: Improved Stability, Reproducibility and High Efficiency. *Energy Environ. Sci.* **2016**, *9*, 1989.
(30) Saliba, M.; Matsui, T.; Domanski, K.; Seo, J. Y.; Ummadisingu, A.; Zakeeruddin, S. M.; Correa-Baena, J. P.; Tress, W. R.; Abate, A.; Hagfeldt, A.; Grätzel, M. Incorporation of Rubidium Cations into Perovskite Solar Cells Improves Photovoltaic Performance. *Science* **2016**, *354*, 206−209.
(31) Abdi-Jalebi, M.; Andaji-Garmaroudi, Z.; Cacovich, S.; Stavrakas, C.; Philippe, B.; Richter, J. M.; Alsari, M.; Booker, E. P.; Hutter, E. M.; Pearson, A. J.; Lilliu, S.; Savenije, T. J.; Rensmo, H.; Divitini, G.; Ducati, C.; Friend, R. H.; Stranks, S. D. Maximizing and Stabilizing Luminescence from Halide Perovskites with Potassium Passivation. *Nature* **2018**, *555*, 497−501.
(32) Zhu, S.; Yao, X.; Ren, Q.; Zheng, C.; Li, S.; Tong, Y.; Shi, B.; Guo, S.; Fan, L.; Ren, H.; Wei, C.; Li, B.; Ding, Y.; Huang, Q.; Li, Y.; Zhao, Y.; Zhang, X. Transparent Electrode for Monolithic Perovskite/Silicon-Heterojunction Two-Terminal Tandem Solar Cells. *Nano Energy* **2018**, *45*, 280−286.
(33) Saliba, M.; Matsui, T.; Seo, J.-Y.; Domanski, K.; Correa-Baena, J. P.; Nazeeruddin, M. K.; Zakeeruddin, S. M.; Tress, W.; Abate, A.; Hagfeldt, A.; Grätzel, M. Cesium-Containing Triple Cation Perovskite Solar Cells: Improved Stability, Reproducibility and High Efficiency. *Energy Environ. Sci.* **2016**, *9*, 1989−1997.
(34) Kim, H. D.; Ohkita, H.; Benten, H.; Ito, S. Photovoltaic Performance of Perovskite Solar Cells with Different Grain Sizes. *Adv. Mater.* **2016**, *28*, 917−922.
(35) Grill, I.; Handloser, K.; Hanusch, F. C.; Giesbrecht, N.; Bein, T.; Docampo, P.; Handloser, M.; Hartschuh, A. Controlling Crystal Growth by Chloride-Assisted Synthesis: Towards Optimized Charge Transport in Hybrid Halide Perovskites. *Sol. Energy Mater. Sol. Cells* **2017**, *166*, 269−275.
(36) Yang, G.; Wang, C.; Lei, H.; Zheng, X.; Qin, P.; Xiong, L.; Zhao, X.; Yan, Y.; Fang, G. Interface Engineering in Planar Perovskite Solar Cells: Energy Level Alignment, Perovskite Morphology Control and High Performance Achievement. *J. Mater. Chem. A* **2017**, *5*, 1658−1666.
(37) Bi, D.; Tress, W.; Dar, M. I.; Gao, P.; Luo, J.; Renevier, C.; Schenk, K.; Abate, A.; Giordano, F.; Baena, J. P. C.; Decoppet, J.-D.; Zakeeruddin, S. M.; Nazeeruddin, M. K.; Grätzel, M.; Hagfeldt, A. Efficient Luminescent Solar Cells based on Tailored Mixed-Cation Perovskites. *Sci. Adv.* **2016**, *2*, No. e1501170.
(38) Wang, Y.; Li, J.; Li, Q.; Zhu, W.; Yu, T.; Chen, X.; Yin, L. a.; Zhou, Y.; Wang, X.; Zou, Z. PbI_2 Heterogeneous-Cap-Induced Crystallization for an Efficient $CH_3NH_3PbI_3$ Layer in Perovskite Solar Cells. *Chem. Commun.* **2017**, *53*, 5032−5035.
(39) Jiang, Q.; Chu, Z.; Wang, P.; Yang, X.; Liu, H.; Wang, Y.; Yin, Z.; Wu, J.; Zhang, X.; You, J. Planar-Structure Perovskite Solar Cells with Efficiency beyond 21%. *Adv. Mater.* **2017**, *29*, 1703852.
(40) Ge, J.; Ling, Z. P.; Wong, J.; Stangl, R.; Aberle, A. G.; Mueller, T. Analysis of Intrinsic Hydrogenated Amorphous Silicon Passivation Layer Growth for Use in Heterojunction Silicon Wafer Solar Cells by Optical Emission Spectroscopy. *J. Appl. Phys.* **2013**, *113*, 234310.
(41) Macco, B.; Melskens, J.; Podraza, N. J.; Arts, K.; Pugh, C.; Thomas, O.; Kessels, W. M. M. Correlating the Silicon Surface Passivation to the Nanostructure of Low-Temperature a-Si: H after Rapid Thermal Annealing. *J. Appl. Phys.* **2017**, *122*, 035302.
(42) Wang, F.; Zhang, X.; Wang, L.; Jiang, Y.; Wei, C.; Xu, S.; Zhao, Y. Improved Amorphous/Crystalline Silicon Interface Passivation for Heterojunction Solar Cells by Low-Temperature Chemical Vapor Deposition and Post-Annealing Treatment. *Phys. Chem. Chem. Phys.* **2014**, *16*, 20202−20208.
(43) Santbergen, R.; Mishima, R.; Meguro, T.; Hino, M.; Uzu, H.; Blanker, J.; Yamamoto, K.; Zeman, M. Minimizing Optical Losses in Monolithic Perovskite/C-Si Tandem Solar Cells with a Flat Top Cell. *Opt. Express* **2016**, *24*, A1288−A1299.
(44) Mei, A.; Li, X.; Liu, L.; Ku, Z.; Liu, T.; Rong, Y.; Xu, M.; Hu, M.; Chen, J.; Yang, Y.; Grätzel, M.; Han, H. A Hole-Conductor-Free, Fully Printable Mesoscopic Perovskite Solar Cell with High Stability. *Science* **2014**, *345*, 295−298.
(45) Ye, S.; Rao, H.; Zhao, Z.; Zhang, L.; Bao, H.; Sun, W.; Li, Y.; Gu, F.; Wang, J.; Liu, Z.; Bian, Z.; Huang, C. A Breakthrough Efficiency of 19.9% Obtained in Inverted Perovskite Solar Cells by Using an Efficient Trap State Passivator Cu(thiourea)I. *J. Am. Chem. Soc.* **2017**, *139*, 7504−7512.

DOI: 10.1021/acsaem.8b00926
ACS Appl. Energy Mater. 2019, 2, 243−249